Supplementary Information

Highly sensitive colorimetric detection and effective adsorption of phosphate based on MOF-808(Zr/Ce)

Yuzhu Zhai[a,b], Yijing Li[a,b]*, Qin Hou[a,b], Yuanhong Zhang[a,b], Enlong Zhou[a,b], Houshen Li[a,b]*, and Shiyun Ai[a,b]

[a] College of Chemistry and Material Science, Shandong Agricultural University, Taian, Shandong, 271018, PR China.

[b] Key Laboratory of Agricultural Film Application of Ministry of Agriculture and Rural Affairs, Taian, Shandong 271018, PR China.

[*] Corresponding authors.

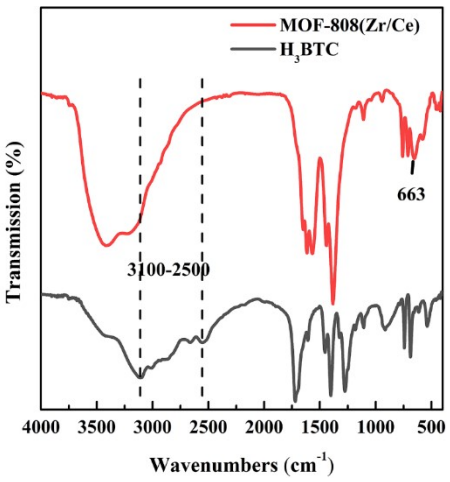

Fig. S1 FTIR spectra of H_3BTC and MOF-808(Zr/Ce).

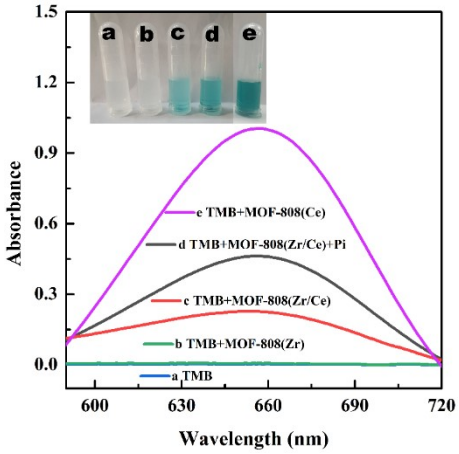

Fig. S2 UV–vis spectra of (a) TMB solution, (b) TMB + MOF-808(Zr) solution, (c) TMB + MOF-808(Zr/Ce) solution, (d) TMB + MOF-808(Zr/Ce) solution + phosphate solution, (e) TMB + MOF-808(Ce) solution. (Reaction conditions: TMB concentration: 186 μM; catalyst: 279 mg mL^{-1}; incubation time: 10 min).

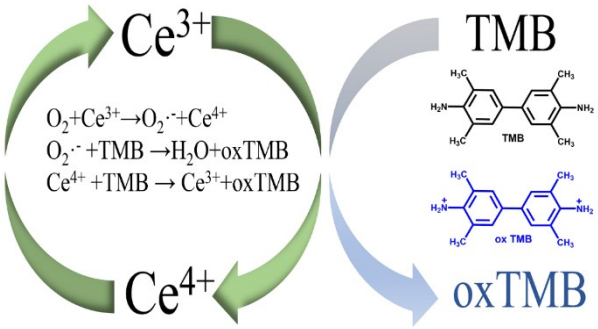

Fig. S3 The underlying process for MOF-808(Zr/Ce) catalyze oxidize TMB reaction.

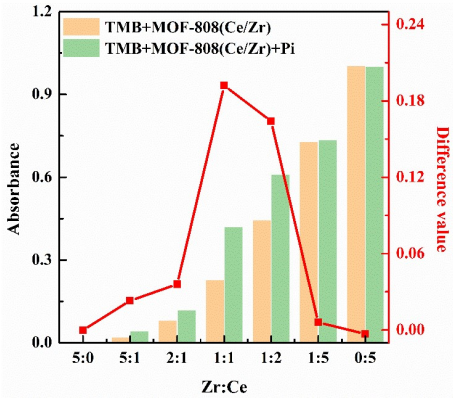

Fig. S4 Effect of the ratio of Zr^{4+}/Ce^{4+} for phosphate detection. The left Y-axis represent A_{654} of the mixture in the absence and presence of phosphate The right Y-axis represent A_{pi}-A_0 (A_{pi} : A_{654} in the presence of phosphate; A_0: A_{654} in the absence of phosphate.).

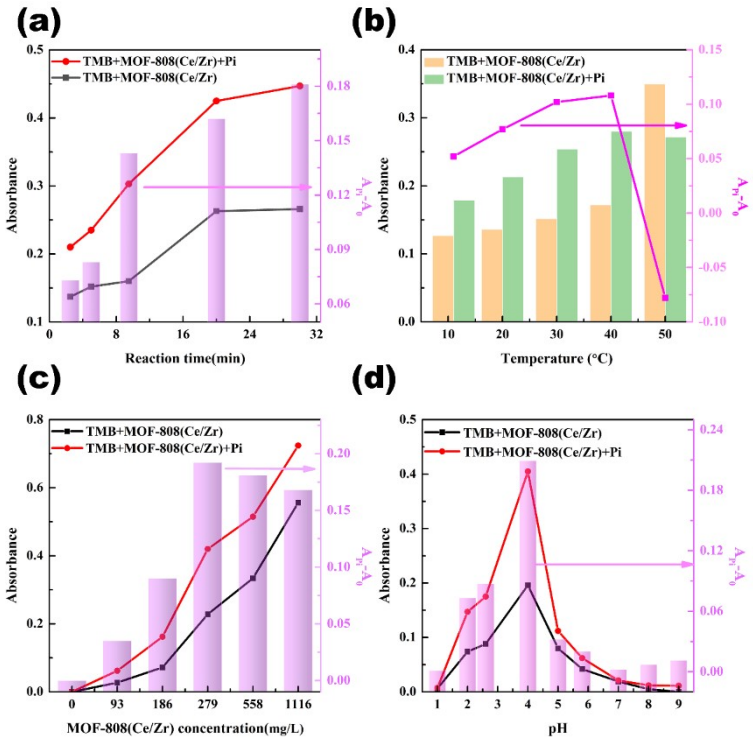

Fig. S5 Effect of (a) reaction time, (b) incubate temperature, (c) catalysts concentration, and (d) pH for Pi detection. The left Y-axis represent A_{654} of the mixture in the absence and presence of Pi. The right Y-axis represent A_{pi}-A_0 (A_{pi} : A_{654} in the presence of Pi; A_0: A_{654} in the absence of Pi.). Reaction conditions: concentration of TMB is 186 μM.

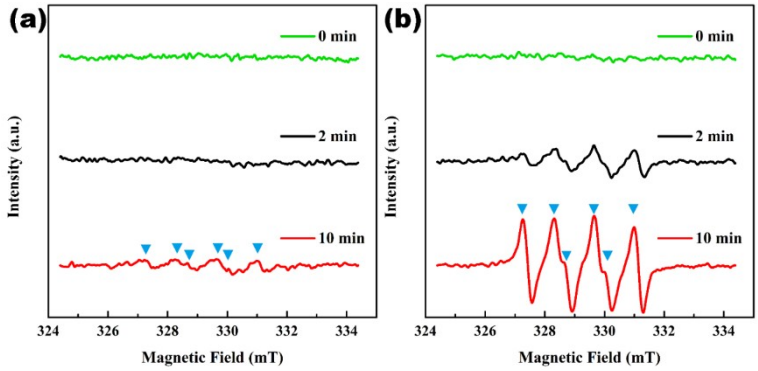

Fig. S6 EPR spectra of MOF-808(Zr/Ce) (a) in the absence and (b) in the presence of phosphate.

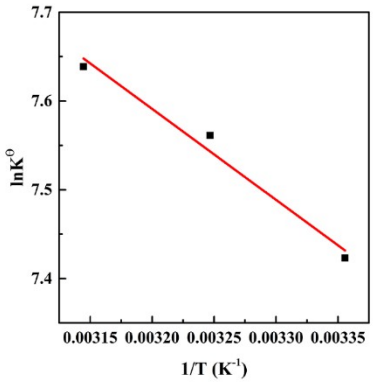

Fig. S7 Phosphate adsorption plot of lnK^{Θ} versus 1/T for estimation of thermodynamic parameters.

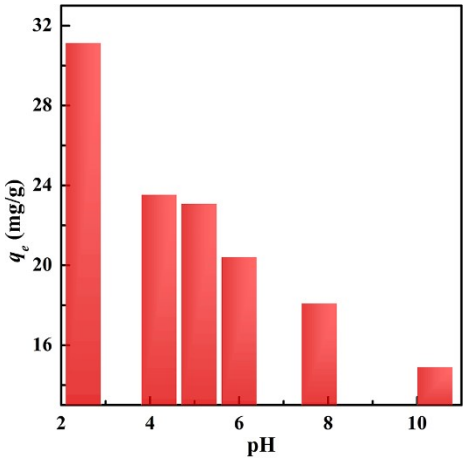

Fig. S8 Effects of the pH on phosphate adsorption of MOF-808(Zr/Ce). The initial pH value is 2.5, 4.2, 6, 7.8, and 10.4. The pH value is 5.1 when the concentration of Pi is 50 mg L^{-1}.

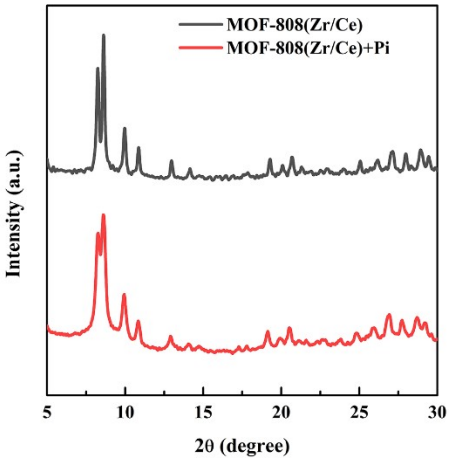

Fig. S9 XRD spectra of MOF-808(Zr/Ce) and MOF-808(Zr/Ce) +Pi.

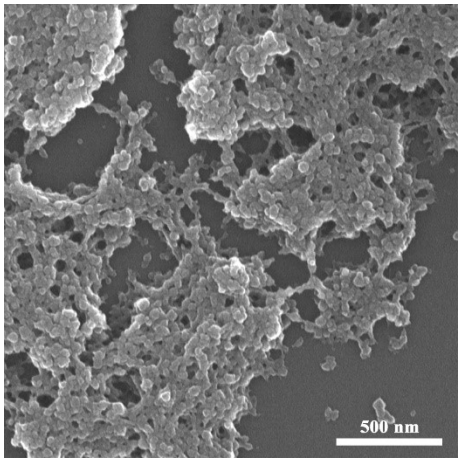

Fig. S10 SEM image of MOF-808(Zr/Ce) after phosphate adsorption.

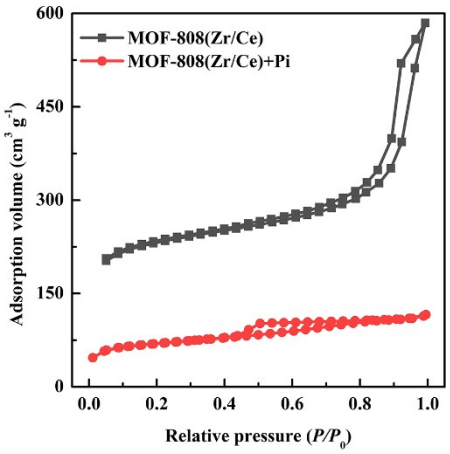

Fig. S11 BET isotherms of MOF-808(Zr/Ce) before and after phosphate adsorption.

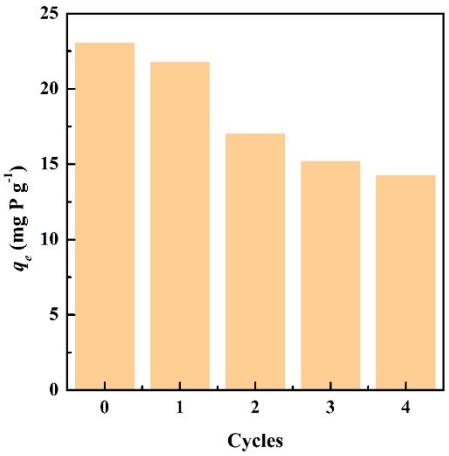

Fig. S12 Reusability of MOF-808(Zr/Ce) for P (50 mg·L^{-1}, 10 h) adsorption from water after NaOH washing.

Table S1 EDS elemental analysis of MOF-808(Zr/Ce).

Element	Atomic %			Mean %
	1	2	3	
C	41.49	47.35	45.83	44.89
O	43.47	41.11	41.22	41.93
Zr	8.48	6.33	7.02	7.28
Ce	6.56	5.22	5.92	5.90

Table S2 List of phosphate detection performance by different material and method.

Material	Method	Linear range (μM)	LOD (μM)	Ref.
MS-Ag nanoplates	Colorimetric	6.1-183	2	1
Eu/Ce/UiO-66-$(COOH)_2$	Fluorescent	0.3-20	0.247	2
Mn-ZnS-QDs/Ce^{3+} nanohybrids	Fluorescent	8-320	2.71	3
Au NPs-CTAB	Luminescence	11.7-750	3.8	4
Reagentless paper-based	Electrochemical	Up to 300	4	5
Oxidized UiO-66(Ce/Zr)	Colorimetric	33.3-666.7	11.1	6
MOF-808(Zr/Ce)	Colorimetric	11-581	3.7	This work

Table S3 Kinetic model parameters of MOF-808(Zr/Ce) for phosphate adsorption.

Kinetic models parameters	
Pseudofirst-order kinetic	
q_e(mg g^{-1})	14.9
k_1 (min^{-1})	0.0089
R^2	0.974
Pseudosecond-order kinetic	
q_e (mg g^{-1})	23.7
k_2 (g mg^{-1} min^{-1})	0.0017
R^2	0.9990
Intraparticle diffusion kinetic	
$k_{p,1}$ (g mg^{-1} min$^{-1/2}$)	1.70333
R^2	0.95966
$k_{p,2}$ (g mg^{-1} min$^{-1/2}$)	0.56232
R^2	0.94611
$k_{p,3}$ (g mg^{-1} min$^{-1/2}$)	0.00888
R^2	0.67726

Table S4 Parameters of isotherm models of MOF-808(Zr/Ce) for phosphate adsorption.

Isotherm models parameters	298 K	308 K	318 K
Langmuir	298 K	308 K	318 K
q_m (mg g^{-1})	54.9	65.1	68.5
K_L (L mg^{-1})	0.054	0.062	0.070
R^2	0.97966	0.98239	0.98202
Freundlich	298 K	308 K	318 K
K_F ((mg·g^{-1}) · (L mg^{-1})$^{1/n}$)	9.60	11.42	13.28
$1/n$	0.35	0.36	0.34
R^2	0.95616	0.96441	0.97442
Temkin	298 K	308 K	318 K
B_T	10.21	12.18	11.88
K_T (L mg^{-1})	0.89	1.03	1.43
b_T (J mol^{-1})	242.68	211.25	222.56
R^2	0.91992	0.92963	0.92836

Table S5 Thermodynamic parameters of phosphate adsorption onto MOF-808(Zr/Ce).

T (K)	K^{Θ}	ΔG^{Θ} (kJ mol^{-1})	ΔH^{Θ} (kJ mol^{-1})	ΔS^{Θ} (J mol$^{-1}\cdot$K^{-1})
298	1674	-9.91		
308	1922	-10.52	8.52	61.83
318	2077	-11.14		

Table S6 Adsorption capacity of phosphate on MOF-808(Zr/Ce) and other adsorbents.

Adsorbent	q_e (mg P g^{-1})	pH	Temperature (°C)	Reference
Fe_3O_4/lignin bio-activated carbons	21.18	7	25	[7]
La/Fe_3O_4-BC	10.82	6.5	25	[8]
NH_2-MIL-100(Fe)	32.14	7	20	[9]
Fe_3O_4@MgAl-LDH@La$(OH)_3$	66.5	7	25	[10]
UiO-66-NH_2	50.5	5.5	40	[11]
MOF-808(Zr/Ce)	54.9	5.1	25	This work

Reference

[1] C. Pinyorospathum, P. Rattanarat, S. Chaiyo, W. Siangproh, and O. Chailapakul, Colorimetric sensor for determination of phosphate ions using anti-aggregation of 2-mercaptoethanesulfonate-modified silver nanoplates and europium ions, *Sensor. Actuat. B-Chem.*, 2019, **290**, 226-232.

[2] C. Gong, Z. Li, G. Liu, and S. Pu, Ratiometric fluorescent sensing for phosphate based on Eu/Ce/UiO-66-$(COOH)_2$ nanoprobe, *Spectrochim. Acta A*, 2021, **252**, 119493.

[3] J. Qin, D. Li, Y. Miao, and G. Yan, Detection of phosphate based on phosphorescence of Mn doped ZnS quantum dots combined with cerium(iii), *RSC Adv.*, 2017, **7**, 46657-46664.

[4] A .A. Fadhel, M. Johnson, K. Trieu, E. Koculi, and A. D. Campiglia, Selective nano-sensing approach for the determination of inorganic phosphate in human urine samples, *Talanta*, 2017, **164**, 209-215.

[5] S. Cinti, D. Talarico, G. Palleschi, D. Moscone, F. Arduini, Novel reagentless paper-based screen-printed electrochemical sensor to detect phosphate, *Anal. Chim. Acta*, 2016, **919**, 78-84.

[6] X. Li, X. Niu, P. Liu, X. Xu, D. Du, and Y. Lin, High-performance dual-channel ratiometric colorimetric sensing of phosphate ion based on target-induced differential oxidase-like activity changes of Ce-Zr bimetal-organic frameworks, *Sensor. Actuat. B-Chem.*, 2020, **321**, 128546.

[7] T. Han, X. Lu, Y. Sun, J. Jiang, W. Yang, and P. G. Jonsson, Magnetic bio-activated carbon production from lignin via a streamlined process and its use in phosphate removal from aqueous solutions, *Sci. Total Environ.*, 2020, **708**, 135069.

[8] L. Wang, J. Wang, C. He, W. Lyu, W. Zhang, W. Yan, and L. Yang, Development of rare earth element doped magnetic biochars with enhanced phosphate adsorption performance, *Colloid. Surface. A*, 2019, **561**, 236-243.

[9] Q. Xie, Y. Li, Z. Lv, H. Zhou, X. Yang, J. Chen, and H. Guo, Effective Adsorption and Removal of Phosphate from Aqueous Solutions and Eutrophic Water by Fe-based MOFs of MIL-101, *Sci. Rep.*, 2017, **7**, 3316.

[10] Z. Lin, and J. Chen, Magnetic Fe_3O_4@MgAl-LDH@$La(OH)_3$ composites with a hierarchical core-shell structure for phosphate removal from wastewater and inhibition of labile sedimentary phosphorus release, *Chemosphere*, 2021, **264**, 128551.
[11] X. Zhang, M. Liu, and R. Han, Adsorption of phosphate on UiO-66-NH_2 prepared by a green synthesis method, *J. Environ. Chem. Eng.*, 2021, **9**, 106672.